JOURNAL OF AIRCRAFT
Vol. 47, No. 6, November–December 2010

Lift Enhancement of Flapping Airfoils by Generalized Pitching Motion

Harish Gopalan*
University of Wyoming, Laramie, Wyoming 82071
and
Alex Povitsky†
University of Akron, Akron, Ohio 44325-3903

DOI: 10.2514/1.47219

The pitching and plunging motions of airfoils have received a lot of attention recently, due to the increased interest in the design of micro air vehicles. The use of combined pitch–plunge motion with phase difference between them has often been used for the generation of thrust and lift. These aerodynamic forces could be significantly enhanced under similar operating conditions by using generalized pitch motion with variable center of wing rotation. The current study investigated the flowfield and aerodynamic forces for this generalized pitching motion. Two-dimensional rigid airfoils were taken as prototypes of micro air vehicle wings. First, the computational results were compared with the available measurements for an SD 7003 airfoil in pure-pitch and pure-plunge motions at $Re = 10,000$. Good agreement was observed between the numerical computations and the experimental results in terms of streamwise velocity, location of the vorticity contours, and wake profiles. Next, the pure-pitch case was considered with the stationary centers of rotation located at different positions along the chord of the airfoil. It was found that the maximum value of the computed average coefficient of lift was obtained when the pitching axis was positioned at either the leading edge or the trailing edge. The generalized pitching motion computations were performed next. It was observed that a phase difference of 90 deg between the pitching motion and the motion of the axis caused a twofold increase of the mean coefficient of lift compared to the pitching about leading edge and combined pitch–plunge motion with a 90 deg phase difference. The stability of the leading-edge vortex was found to be responsible for the enhancement of lift by reduction in pressure at the upper surface of the airfoil. However, thrust force was not generated by applying the generalized pitching alone, whereas it was generated by the combined pitch–plunge motion. Finally, a generalized pitching motion combined with a superimposed plunging motion was studied. It was found that for this motion, thrust was generated and the generated lift was higher than that for the generalized pitching motion. This result may help in the use of superposition of kinematic motions of wings to produce the desired amount of lift and thrust.

Nomenclature

C_L, $\bar{C}_L$	=	instantaneous and average coefficient of lift
C_p	=	coefficient of pressure, $(p - p_o)/(0.5\rho U_\infty^2)$
c	=	chord of the airfoil
h	=	plunging amplitude
h_e	=	maximum distance traveled by leading or trailing edge during pitching motion
k	=	reduced frequency
$p - p_o$	=	gauge pressure.
Re	=	Reynolds number, $U_\infty c/\nu$
T	=	time period of motion
t	=	nondimensional time (nondimensionalized by c/U_∞)
U_∞	=	freestream velocity
x^*, y^*	=	coordinates at $t = 0$
$x(t)$, $y(t)$	=	translational motion of the airfoil (nondimensionalized by c)
x_c, y_c	=	center of rotation for pure pitching and generalized pitching
$\theta(t)$	=	rotational motion of the airfoil
θ_0, θ_a	=	pure-pitch amplitude and freestream angle of attack
ϕ	=	phase difference

Presented as Paper 2008-6394 at the 26th AIAA Applied Aerodynamics Conference, Honolulu, HI, 18–21 August 2008; received 16 September 2009; revision received 29 July 2010; accepted for publication 30 July 2010.

*Postdoctoral Associate, Department of Mathematics; hgopalan@uwyo.edu. Member AIAA.

†Associate Professor, Department of Mechanical Engineering; povitsky@uakron.edu. Senior Member AIAA (Corresponding Author).

I. Introduction

THE superior flight characteristics exhibited by birds and insects with a wingspan at or below 15 cm can be taken as a prototype of the most perfect form of flying machine ever created. Birds and insects achieve the aerodynamic performance of their flight by the flapping motion of their wings and successfully overcome the wind shear and gust conditions. The understanding of the flapping-wing aerodynamics and its application to the design of micro air vehicles (MAVs) and nano air vehicles has received a lot of attention recently. The size of a MAV and its speed of operation result in relatively low Reynolds number flight (10^4–10^5), which is far below the flying conditions of a conventional fixed-wing aircraft [1,2]. In this flow regime, rigid fixed wings drop dramatically in aerodynamic performance because of flow separation, whereas flexible flapping wings used by small natural fliers [3] do not exhibit a drop in aerodynamic performance. For the above size of wingspan and range of Reynolds numbers, flapping wings have several advantages over fixed wings, such as enhanced lift, low noise, and better maneuverability [1,4–6]. The advance in the microfabrication technology also makes it possible to produce flapping wings at low cost [7]. This has inspired a number of studies to obtain a clear understanding of the aerodynamics of the bird and insect flights [8–11], including the effect of wind gust [12].

The most commonly considered kinematic motions include the pitching about constant axis, plunging motion, or a combination of

both. A combined experimental and numerical study on the equivalence of the angle of attack between the pitching and plunging motions [13] suggested that the pitching motion produces better aerodynamic performance (higher lift and thrust) for the same input power compared to the plunging motion.

Although the motion of flapping wing in nature is rather complex, the MAV literature focus has been on studying combined pitch–plunge motions with fixed axis of rotation. In most combined pitch–plunge motion studies, a properly chosen phase difference introduced between the two separate motions (pitch and plunge) was very important for superior aerodynamic performance. In particular, it has been found that a phase difference of 90 deg between the pitching (rotation about a fixed point at the wing chord) and plunging (rotation about a point at infinity) motions corresponds to the best aerodynamic performance [14–18].

A modified version of the pitching motion (compared to traditional pitching about a fixed axis of rotation) has been investigated in the current study as an attempt to influence both the momentary and period-averaged lift force. Pitching motion with moving axis of rotation is considered. As will be seen from the results obtained in the current research, a pitching motion with a moving axis of rotation performs better in terms of generated lift than a combined pitch–plunge motion if the phase difference between pitching motion and periodic motion of center of rotation is selected properly.

The efficiency of different kinematic motions mentioned before depend on the formation of the leading-edge vortex (LEV) and occurrence of dynamic stall to ensure higher aerodynamic forces generated by flapping wings [1,8,12]. The effect of the magnitude of the leading-edge vortex and balance in creation and transport of vorticity of the LEV are very important to determine the aerodynamic performance of the flight [19]. Therefore, the current study investigates the formation of the leading-edge vortex at Strouhal ($2kh/\pi$) numbers less than 0.15 using the generalized pitching motion and its effect on the aerodynamic forces.

Prior research [20] has shown that higher values of reduced frequencies or amplitudes can result in the increase of lift forces. Our aim is to be able to find kinematic motions to do the same at low values of reduced frequencies and amplitudes by modifying the kinematic motions. At low values of the Strouhal number ($2kh_e/\pi \sim 0.13$, h_e is the maximum distance traveled by leading or trailing

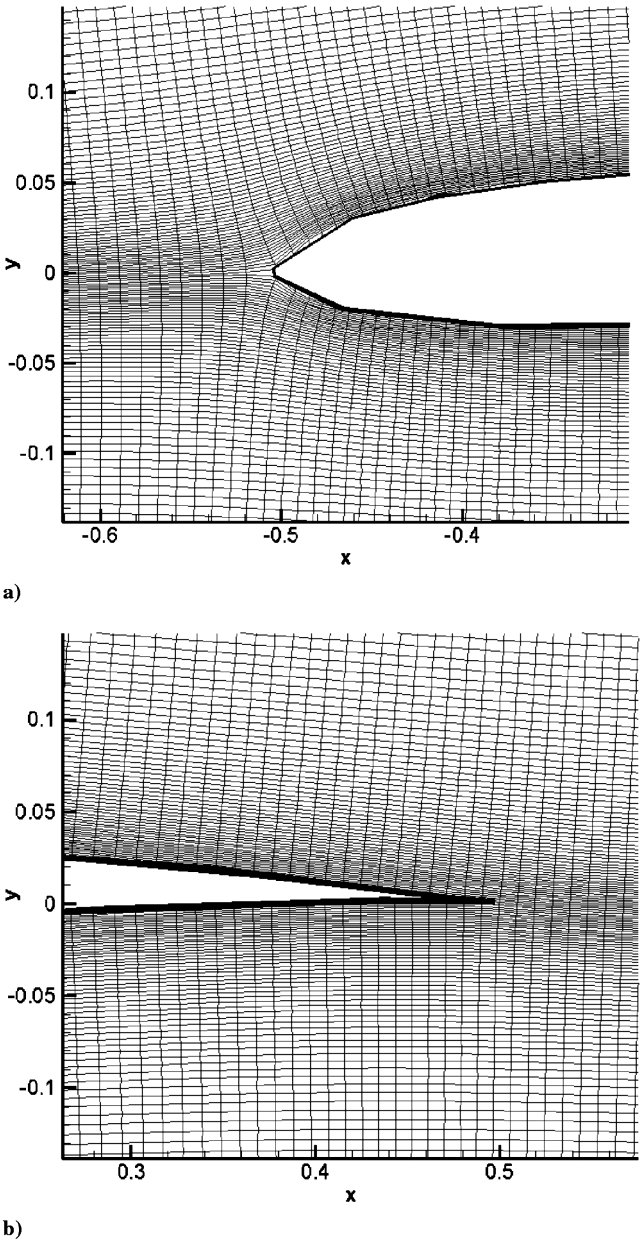

Fig. 1 Numerical grid used for performing the computations: a) leading edge and b) trailing edge (every second line is shown in the figure).

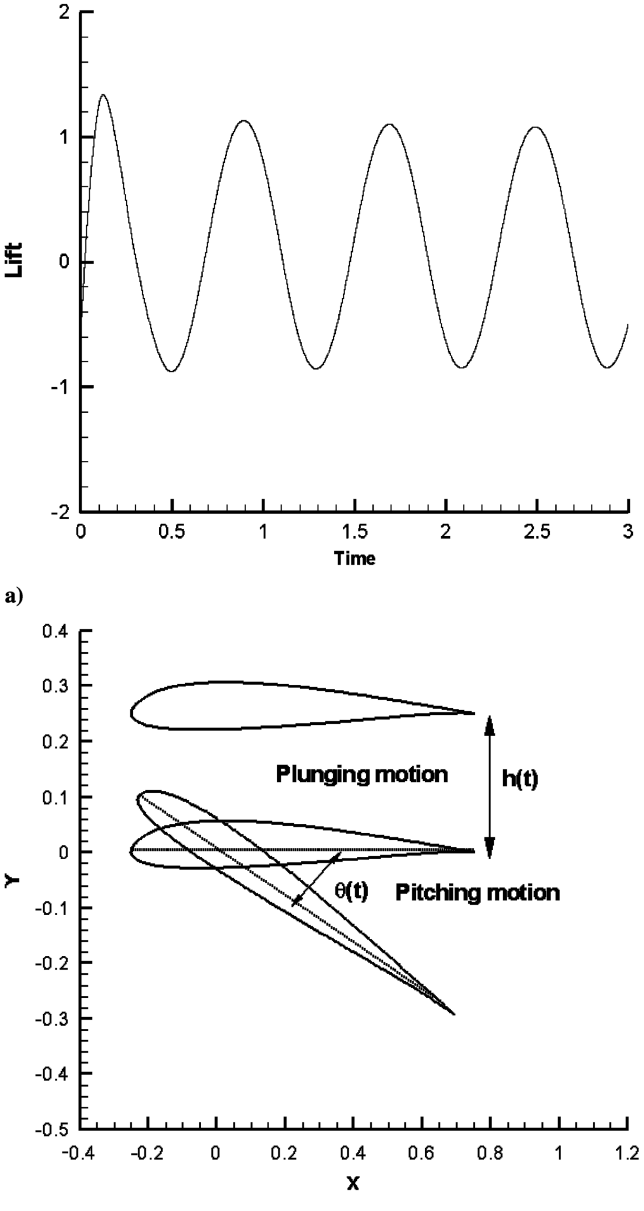

Fig. 2 Periodic motion of the airfoil: a) time history of the coefficient of lift for pitching motion (nondimensional time period is 0.8) and b) pitching and plunging motions of the airfoil (schematic, not to scale).

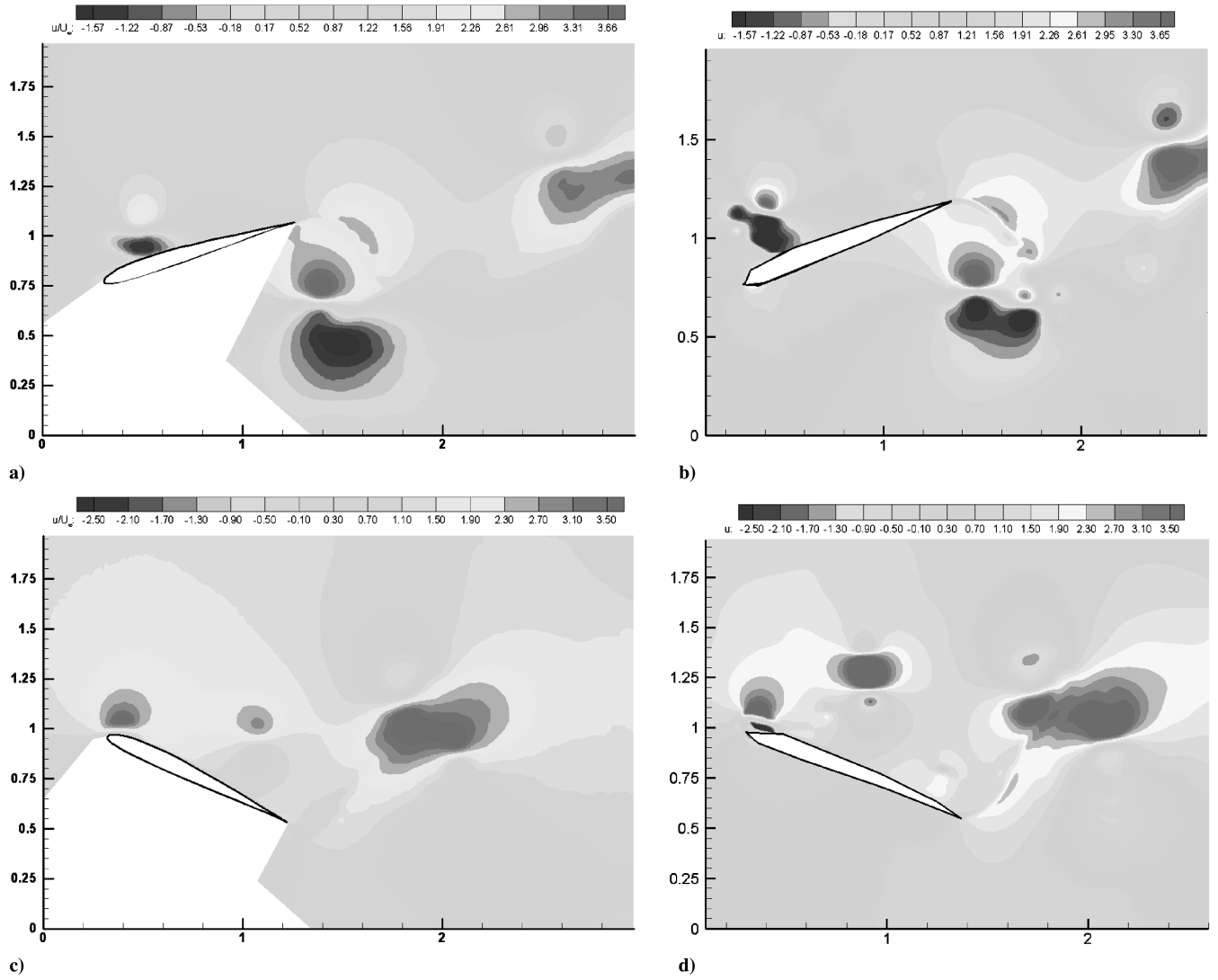

Fig. 3 Comparison of streamwise velocity from experiments and numerical simulation at the top and bottom stroke for an SD 7003 airfoil in pure pitch at $Re = 10,000$: a) bottom stroke: experiment, b) bottom stroke: numerical, c) top stroke: experiment, and d) top stroke: numerical.

edge during pitching motion), the use of the pure-pitching motion generates drag force. To create thrust, a generalized pitching motion combined with plunging motion is proposed and studied. It is found in the current study that for this motion thrust is generated and the generated lift is higher than that for the standalone generalized pitching motion.

The current study is based on numerical solution of Navier–Stokes equations. Numerical results are compared to inviscid quasi-steady results obtained by Garrick [21] and Young [22]. Numerical and approximate analytical results have good matching for regular pitching and plunging motions, but not for the generalized pitching motion. This confirms the need for computational fluid dynamics (CFD) studies of flapping wings with complex kinematics of motion.

The rest of the paper is arranged as follows. The computational model is described in Sec. II. A two-dimensional rigid airfoil model has been used for performing the numerical simulations. The two-dimensional rigid airfoil model was chosen since many previous studies were able to study the flapping motions in nature using two-dimensional analogs [8]. The kinematic motions of the airfoil that have been considered in the current study are introduced in Sec. III. Comparison with experimental results for pitching and plunging motions is presented in Sec. IV to validate the use of a two-dimensional model. The investigation of the generalized pitching motion and combined generalized pitching and plunging motions is presented in Sec. V. Section VI contains the conclusions of the current study and scope for future work.

II. Computational Method

The numerical computations are performed using an unsteady Navier–Stokes solver in a noninertial coordinate system moving with the airfoil [23,24]. Another example of use of a moving grid for flapping-wing motion combined with lower-order of approximation (CFL3D) is presented in [25]. The current solver uses fourth-order compact central differencing for spatial discretization [26], a tenth-order implicit filter [27] to filter the unresolved wave numbers and to avoid numerical oscillations, and a third-order low-storage explicit Runge–Kutta scheme [28] and energy transfer and annihilation [29] boundary condition for absorbing the outgoing waves at the artificial domain boundaries. The numerical grid is generated using streamlines obtained from inviscid potential flow solution [24]. This grid-generating algorithm generates H-grids around curvilinear geometries while ensuring the orthogonality of the generated grid. The method also allows for the easy clustering of points in the boundary layer without sacrificing orthogonality. All the computations have been performed on a 300×100 H-grid. The numerical grid that has been used for performing the computation is shown in Fig. 1 and grid validity is checked in [23,24]. Grid clustering of 15 points across the boundary layer was used. The rigid-body motion of the grid attached to the moving airfoil is adopted to account for the kinematic motion. The outer domain extends to 10 chords on along the streamwise direction and 2–5 chords along the normal direction to the airfoil surface.

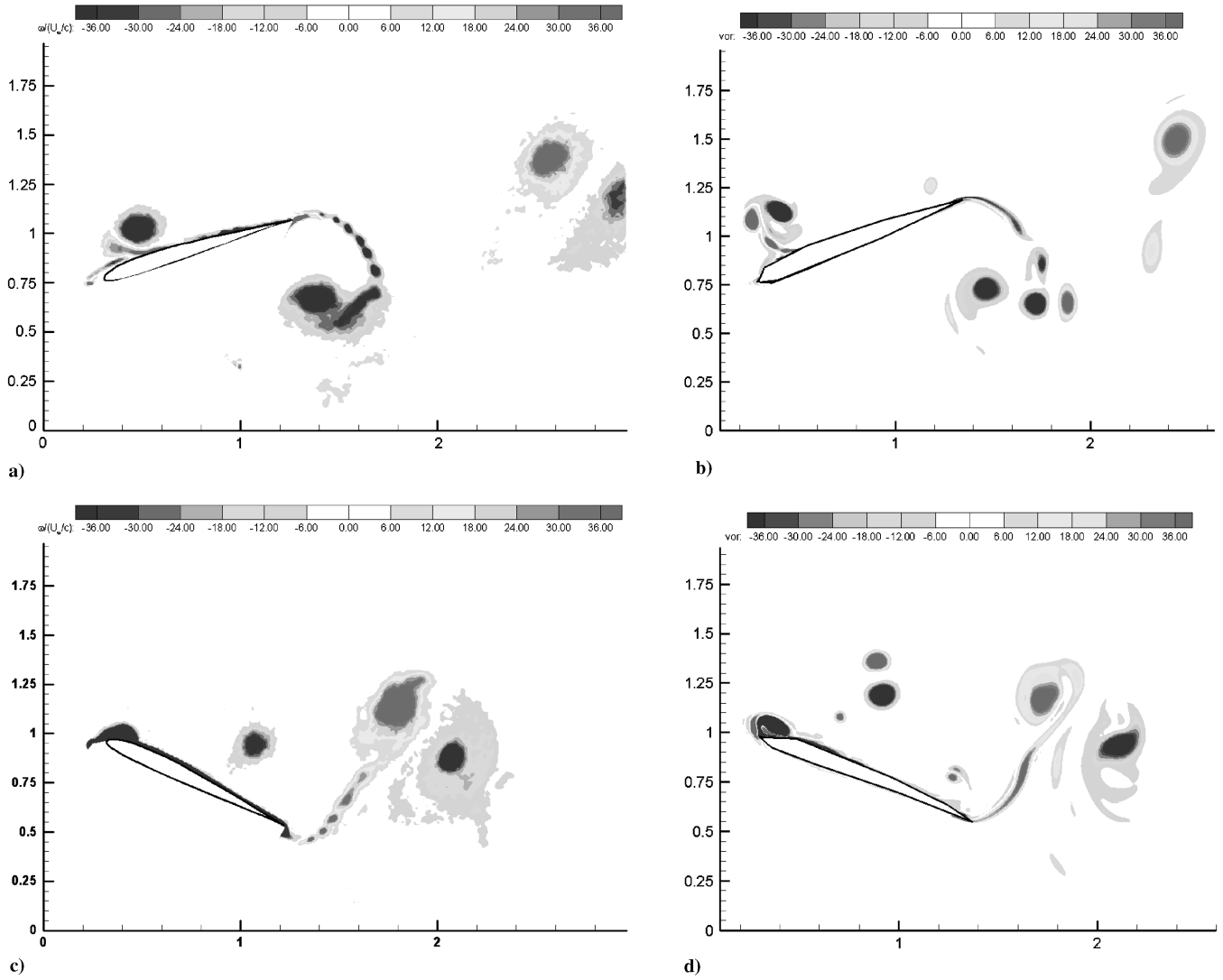

Fig. 4 Comparison of vorticity contours from experiments and numerical simulation at the top and bottom stroke for an SD 7003 in pure pitch at $Re = 10,000$: a) bottom stroke: experiment, b) bottom stroke: numerical, c) top stroke: experiment, and d) top stroke: numerical.

The computations were initialized with a potential velocity field computed for the purpose of grid generation (see above). The initial transient was observed for about one period of motion. The solution turned periodic after the initial transient (see Fig. 2a). To ensure and test that the artificial boundary conditions at the domain boundaries do not cause numerical reflections that contaminate the solution, the computations were run first for 25 periods of motion for the initial test case. All other computations were run for 10 periods of motion. Further details can be found in [23].

III. Airfoil Kinematics

The angular motion $\theta(t)$ and Cartesian coordinates $x(t)$ and $y(t)$ of rigid airfoil (see Fig. 2b) pitching with the fixed center of rotation (lying at the origin of the coordinate system at $x = 0$, and $y = 0$) are given by

$$\theta(t) = \theta_0 \cos(2kt + \phi) + \theta_a, x(t) = x^* \cos(\theta) - y^* \sin(\theta), \quad \text{and}$$
$$y(t) = x^* \sin(\theta) + y^* \cos(\theta) \tag{1}$$

where $k = \omega c/2U_\infty$ is the reduced frequency, θ_0 is the amplitude of the pitching motion, θ_a is the angle of attack of the airfoil in the absence of pitching, ϕ is used to introduce phase difference between combined motions, $\theta_0 \cos(2kt + \phi)$ is a momentary pitching angle, x^* and y^* are the physical coordinates of an arbitrary point at airfoil normalized by the airfoil chord length at $t = 0$, and c is the airfoil chord. The airfoil coordinates for plunging motion are given by

$$x(t) = x^*, \qquad y(t) = h \cos(2kt) \tag{2}$$

where h is the nondimensional plunging amplitude normalized by the airfoil chord length. The kinematic motions for the generalized pitching case are given by

$$x(t) = x_c + (x^* - x_c)\cos(\theta(t)) - (y^* - y_c)\sin(\theta(t))$$
$$y(t) = y_c + (x^* - x_c)\sin(\theta(t)) + (y^* - y_c)\cos(\theta(t))$$
$$x_c = 0.5(1 - \cos(2kt)), \qquad y_c = 0 \tag{3}$$

When $x_c \equiv 0$ and $y_c \equiv 0$, the airfoil performs the pure-pitching motion about a fixed axis [see Eq. (1)].

IV. Comparison with Experiments

Our numerical results obtained for the SD7003 airfoil has been validated against experimental data (see [30]) in which the details of measurements techniques are provided. The SD 7003 airfoil [31] was chosen for the experiments because of the long and stable laminar separation bubble that it exhibits over a broad range of angle of attack and at Reynolds numbers below 100,000 [32]. The comparison of the streamwise velocity contours and the computed vorticity contours with the particle image velocimetry (PIV) measurements presented in [25,30] are shown for the following two cases: 1) pure-pitching motion at $Re = 10,000$, $k = 3.93$, and $\theta(t) = 4^\circ + 21^\circ \cos(2kt)$ and 2) pure-plunging motion at $Re = 10,000$, $k = 3.93$, and

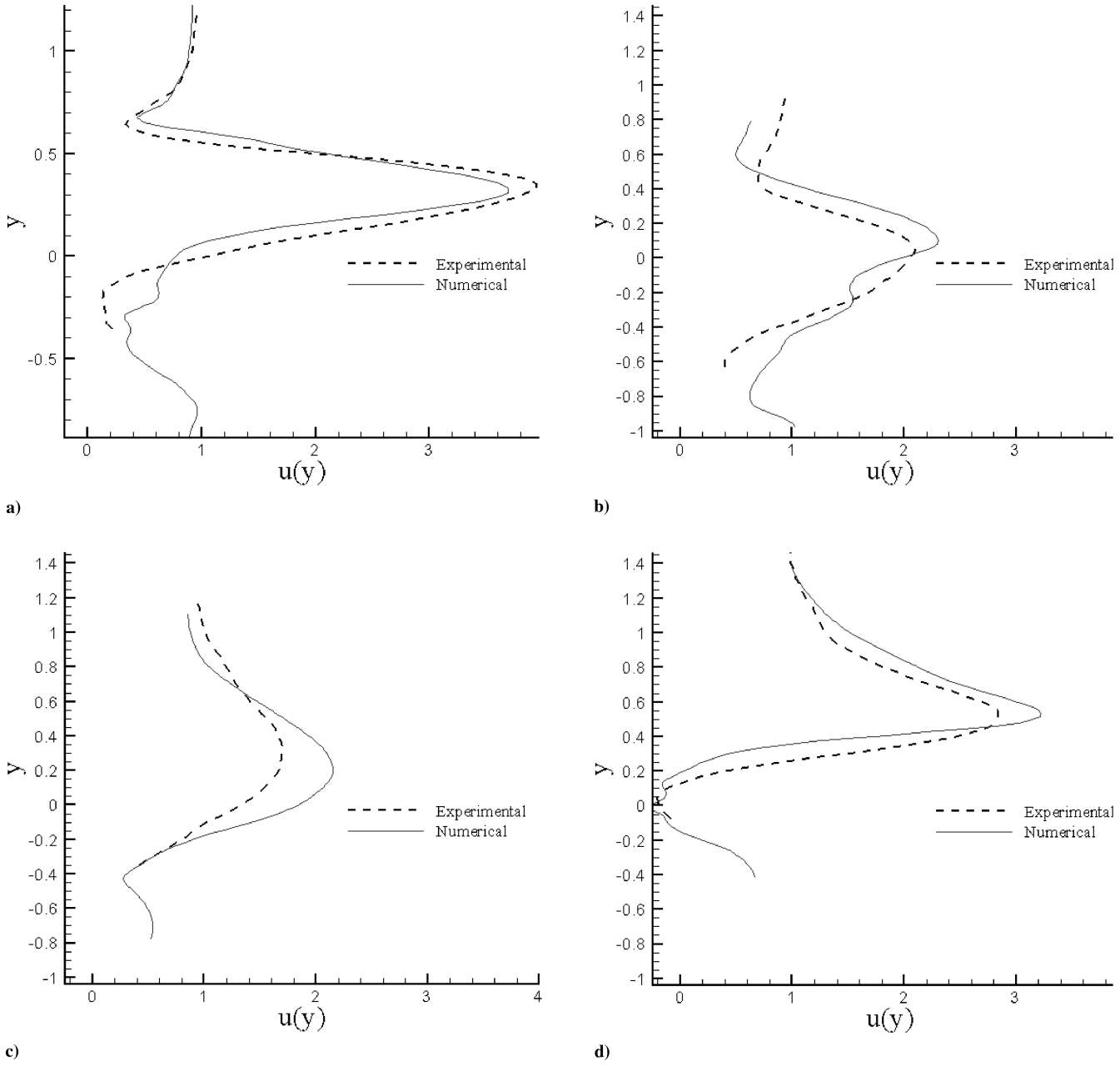

Fig. 5 Comparison of streamwise velocity components for an SD 7003 in pure pitch at $Re = 10,000$ in the wake at one-chord downstream of the trailing edge: a) $T = 0$, b) $T = 1/4$, c) $T = 1/2$, and d) $T = 3/4$.

$y(t) = 0.05\cos(2kt)$. In addition to the above comparisons, comparison between the dye injection and numerical particle tracking is shown for pure plunge at $Re = 10,000$, $k = 7.85$, and $h = 0.05$.

A. Pitching Motion About Fixed Center of Rotation

The comparison between the streamwise velocity contours and vorticity contours during the top and bottom strokes are shown in Figs. 3 and 4, respectively. The center of rotation has been fixed at the quarter-chord location for the present case to match with the experiments. In the PIV there is a mask blanking the shadow of the laser light sheet (data not available in the narrow region below the SD 7003 airfoil in the experiments). There is a good qualitative agreement between the numerical and experimental results. The horizontal and vertical locations of the vortex cores are accurately predicted. The upward motion of the vortex core observed in the experiments has also been accurately captured. The numerical simulations show somewhat higher magnitude of streamwise velocity compared to the experimental measurements in certain regions.

The comparison of the streamwise velocity between the experiments and numerical simulations are shown in Fig. 5, one chord downstream of the trailing edge. For $T = 0$, the numerical streamwise velocity profile in the wake (Fig. 5a) shows a lower magnitude compared to the experiments but the shape of the profile and the width has been captured well. The velocity profile in the wake shows a higher magnitude in the numerical study compared to the experiment and the peaks of the velocity is a bit higher compared to the experiment (Fig. 5b) for $T = 1/4$. Finally, for $T = 1/2$ and 3/4, numerical velocity profile in the wake shows a higher magnitude of the peak compared to the experiments, similar to $T = 1/4$ (Figs. 5c and 5d). Overall, there is a fair agreement between the numerical and experimental profiles.

B. Plunging Motion

Similar to the above pure-pitch case, the velocity and vorticity (see Figs. 6 and 7) show good agreement between experiments and computations in plunging airfoil motion. In particular, the horizontal and vertical locations of the vortex cores showing good corre-

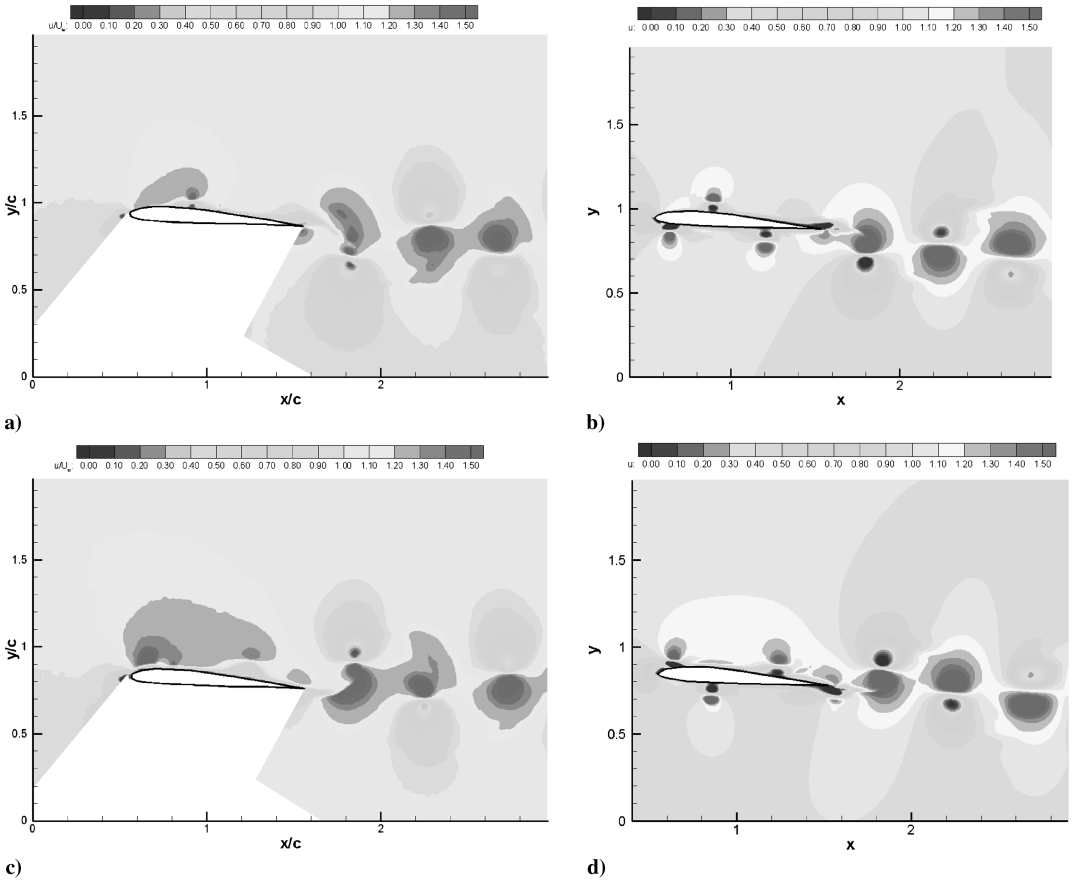

Fig. 6 Comparison of streamwise velocity from experiments and numerical simulation at the top and bottom stroke for an SD 7003 in pure plunge at $Re = 10,000$: a) bottom stroke: experiment, b) bottom stroke: numerical, c) top stroke: experiment, and d) top stroke: numerical.

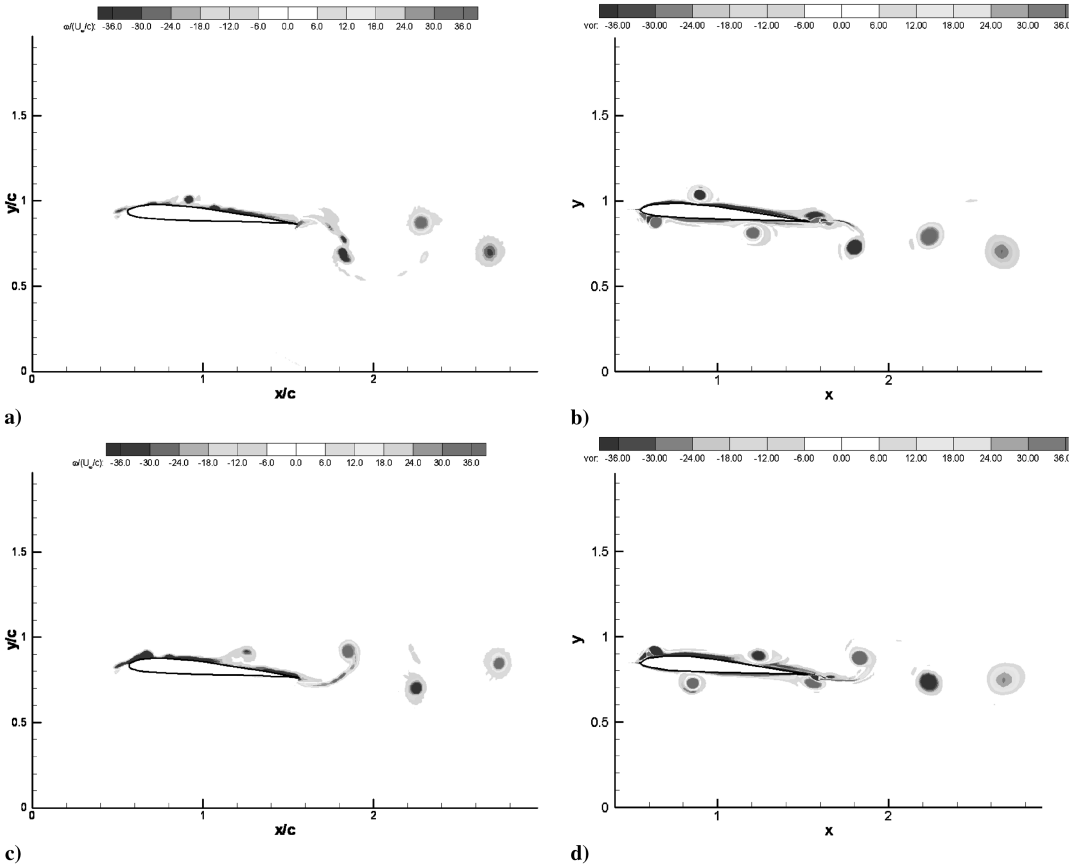

Fig. 7 Comparison of vorticity contours from experiments and numerical simulation at the top and bottom stroke for an SD 7003 in pure plunge at $Re = 10,000$: a) bottom stroke: experiment, b) bottom stroke: numerical, c) top stroke: experiment, and d) top stroke: numerical.

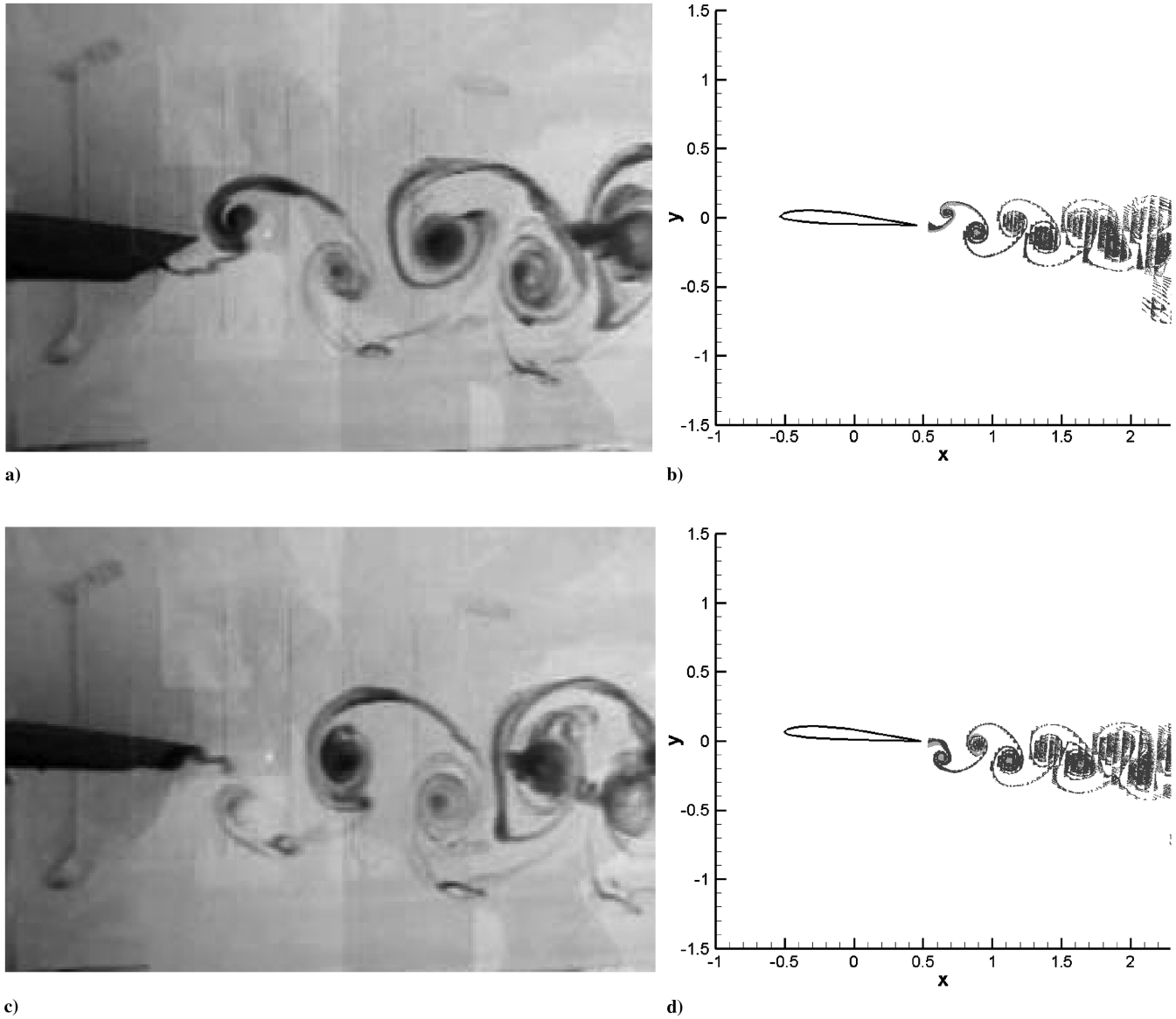

Fig. 8 Comparison between experimental dye injection and numerical particle tracking for an SD 7003 airfoil in pure plunge at $Re = 10,000$, $k = 7.85$, $h = 0.05$: a) bottom stroke: experiment, b) bottom stroke: numerical, c) top stroke: experiment, and d) top stroke: numerical.

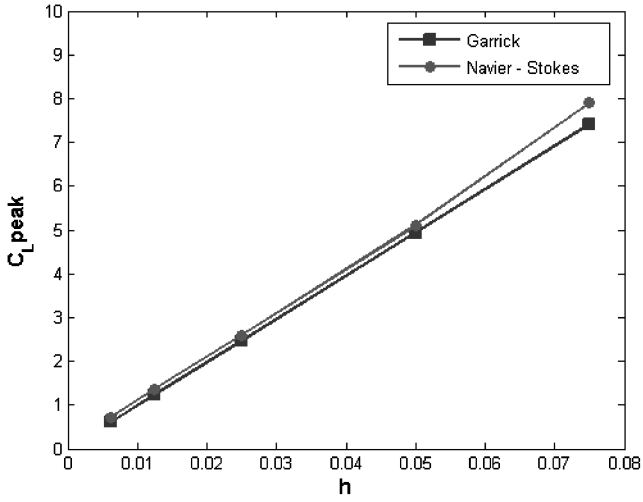

Fig. 9 Comparison of the peak amplitude of the coefficient of lift between the CFD computations and the analytical expression of Garrick [21] and Young [22] for a range of plunging amplitudes.

spondence to the experimental results. The numerical simulations predict a slightly higher magnitude of velocity and vorticity compared to the experimental measurements in some areas. Because of the mask blanking, the regions near the leading and trailing edges cannot be clearly compared. The comparison of the streaklines from experiments and numerical particle tracking (see [23] for details of the particle tracking algorithm) is shown in Fig. 8 for a pure-plunge case at $Re = 10,000$, $k = 7.85$, and $h = 0.05$. A good agreement between the streaklines observed in the dye injection experiment and the numerical particle tracking is observed. The fair agreement between the two-dimensional computational results and the experiments provide encouragement for employing the developed

Table 1 Average coefficient of lift for pure pitch about different fixed axes of rotations

Location of axis of rotation	Average coefficient of lift	Average coefficient of thrust	Quasi-steady lift
Leading edge	0.25	−0.036	0.22
Quarter-chord	0.23	−0.038	0.22
Half-chord	0.21	−0.041	0.22
Trailing edge	0.24	−0.038	0.22

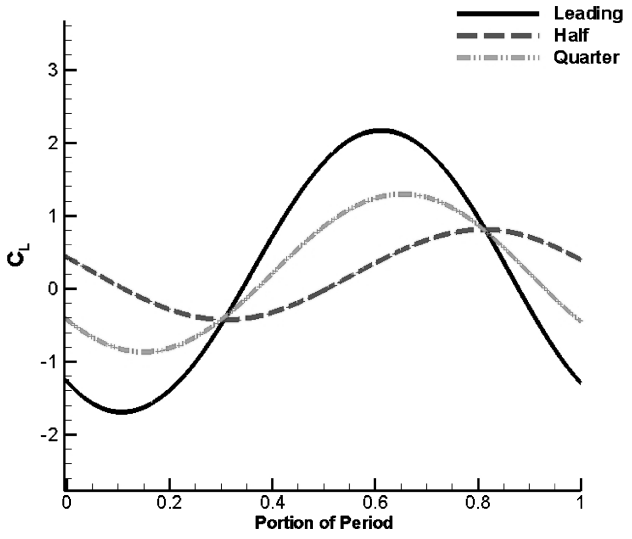

a)

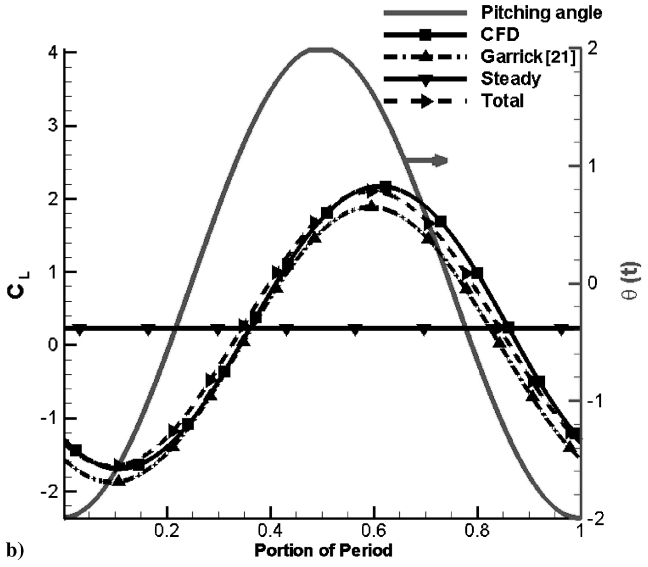

b)

Fig. 10 Instantaneous coefficient of lift for an airfoil in pitching motion: a) pitching axis located at different points along the chord and b) comparison of CFD and quasi-steady results for the pitching about the leading edge. Right arrow indicates that the right vertical axis is used for the plot.

two-dimensional solver for modeling of generalized pitching in the current study.

V. Analysis of Aerodynamic Forces: Generalized Pitching

The computed value of the peak coefficient of lift for the SD 7003 airfoil in pure plunge is compared with the analytical expression of Garrick [21] and Young [22] in Fig. 9 at $Re = 10,000$, and $k = 3.93$, with the varied plunging amplitude $h = 0.05$–0.075. Although the expression of Garrick [21] is strictly valid only for symmetric airfoils, the small value of the Strouhal number ensures that the asymmetry of the airfoil does not significantly affect the predictions. It can be seen from the figure that there is a good agreement between Garrick [21] results and current CFD results.

Next, computations have been performed for an SD 7003 airfoil in pure pitch at $Re = 10,000$ for a reduced frequency and pitching amplitude of 3.93 and 2 deg, respectively. In these computations, a steady-state angle of attack θ_a is set to zero. The angle of attack corresponding to zero lift in steady flight is equal to -2 deg for the SD 7003 airfoil [25]. For the considered pitching amplitude, the

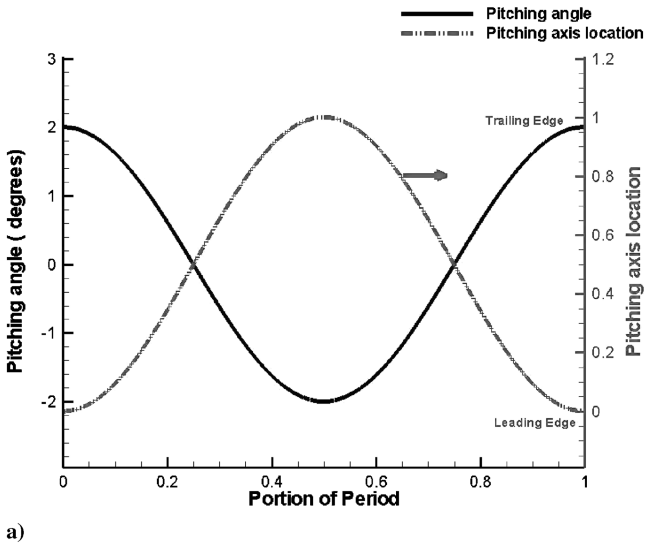

a)

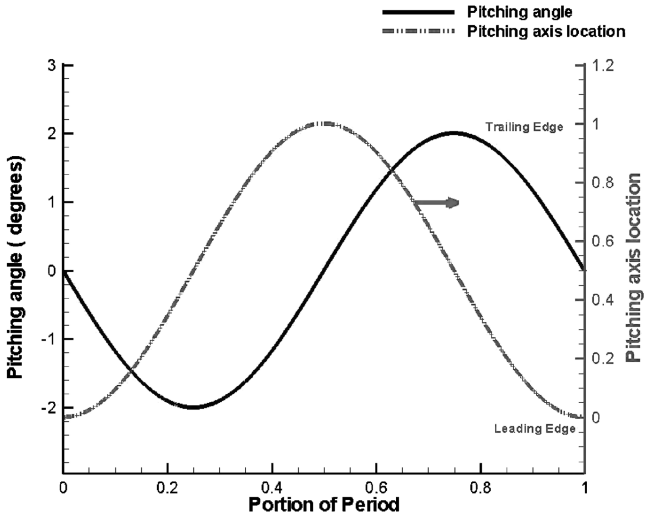

b)

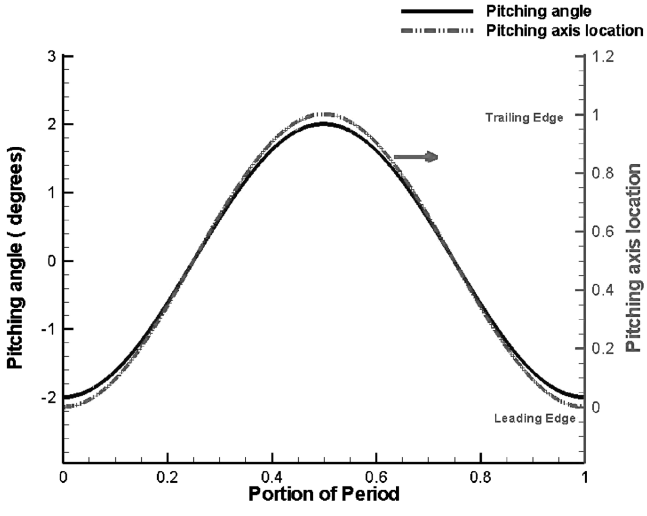

c)

Fig. 11 Kinematic motion for the generalized pitching case: a) MC1, b) MC2, and b) MC3.

momentary steady lift should be always nonnegative, and period-averaged steady lift is equal to 0.22.

The CFD computations were performed for the pitching axis located at different positions (leading edge, the quarter of chord, the

Table 2 Average coefficient of lift for periodically moving center of rotation[a]

Case	Average coefficient of lift	Average coefficient of thrust	ϕ
Pitching about leading edge	0.25	−0.036	0
MC1	0.23	−0.023	0
MC2	0.59	−2e − 4	$\pi/2$
MC3	0.204	−0.028	π
Pitch-plunge	0.27	0.012	$\pi/2$
Pitch-plunge with MC2	0.67	0.007	$\pi/2$

[a]Lift coefficient for pure pitch about the leading edge is presented for comparison.

half-chord, and the trailing edge) along the chord. The computed values of the average coefficient of lift and thrust are shown in Table 1, and the instantaneous coefficient of lift is shown in Fig. 10a for a single period of oscillation. Next, we compare the computed mean and instantaneous values of the coefficient of lift with the results obtained from quasi-steady approximation (see the Appendix). Instantaneous coefficient of lift obtained by CFD was compared to quasi-steady approximations, as shown in Fig. 10b for the case of pitching about the leading edge. In Table 1, coefficient of lift has been averaged over a period and presented for the above-listed locations of pitching axis. It can be seen from Fig. 10b that the quasi-steady approximation shows a good agreement with CFD results. Pitching about the leading edge corresponds to the maximum value of the average coefficient of lift. The peak lift coefficient for the leading-edge rotation point is the maximum because of the largest possible radius of rotation, which is equal to c for the trailing edge. The maximum momentary lift is enhanced by an order of magnitude compared to the steady lift (see Fig. 10b). However, the negative peak left coefficient is also the maximum by magnitude in this case, and therefore the average lift is only moderately increased for this case.

It can be seen from Table 1 that the period-averaged lift for leading-edge location of pitching axis is only 13.6% higher than that generated by the steady angle of incidence. All the cases considered result in drag (see Table 1, where pitching about the leading edge shows minimum drag among considered cases).

Subsequently, computations were performed using the generalized pitching motion at the same Reynolds number, reduced frequency, and pitching amplitude as before. Before proceeding with a discussion of the forces, let us briefly discuss the generalized pitching motion.

In the generalized pitching motion, the coordinate of the momentary axis of pitching moves between leading and trailing

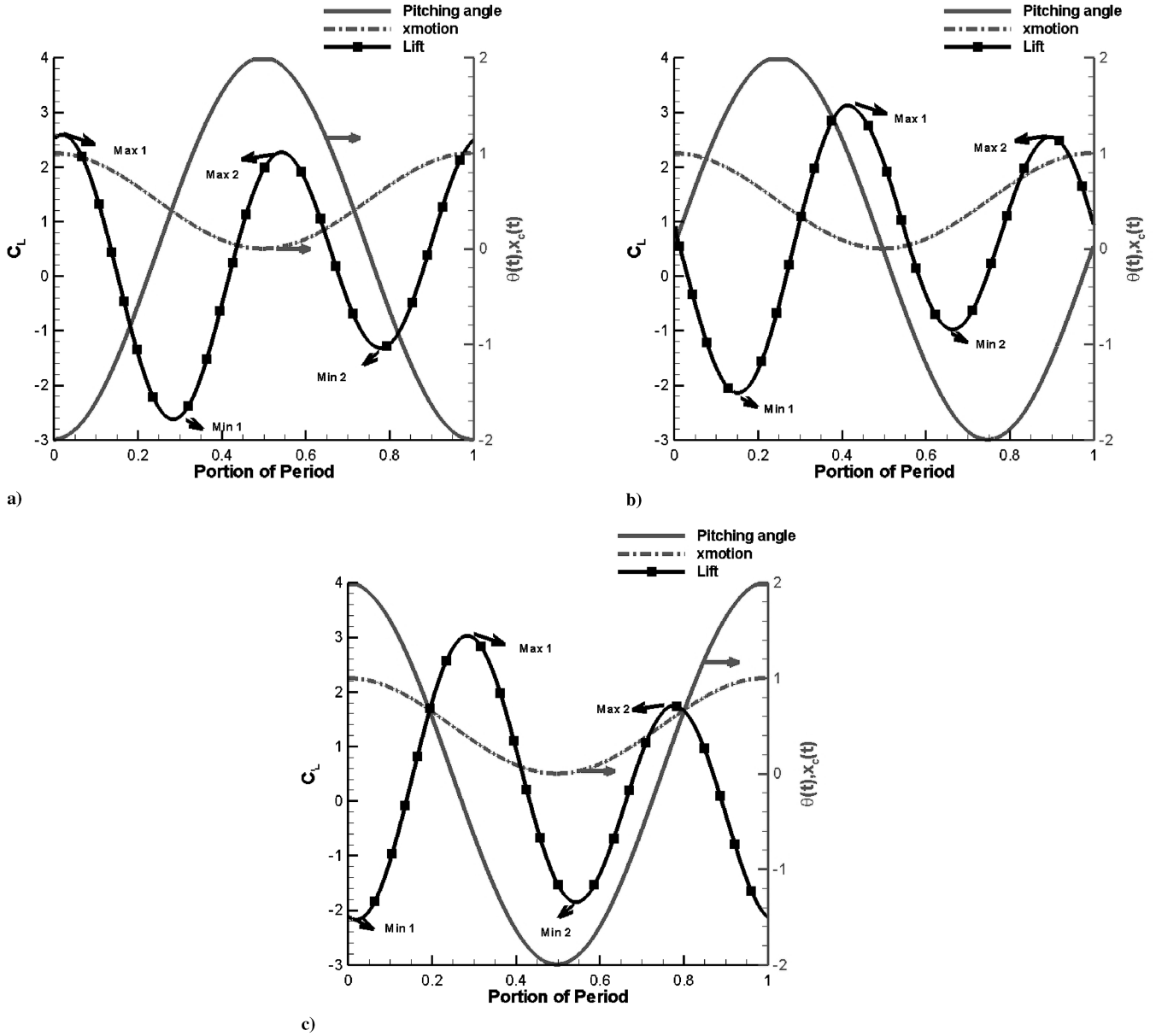

Fig. 12 Plots of the pitching angle, axis motion, and instantaneous coefficient of lift for the generalized pitching case: a) MC1, b) MC2, and c) MC3.

Table 3 Comparison of the location of the primary/secondary maxima/minima for MC1, MC2, and MC3

Location	MC1			MC2			MC3		
	$\theta(t)$, deg	$x_c(t)/c$	$C_L(t)$	$\theta(t)$, deg	$x_c(t)/c$	$C_L(t)$	$\theta(t)$, deg	$x_c(t)/c$	$C_L(t)$
Min 1	0.5	0.38	−2.6	1.6	0.8	−2.14	2	1	−2.2
Min 2	−0.44	0.62	−1.32	−1.74	0.25	−1.0	−2	0	−1.85
Max 1	−2	1	2.6	1	0.06	3.12	−0.5	0.37	3.02
Max 2	2	0.02	2.25	−1.14	0.9	2.54	0.4	0.6	1.74

edges of the airfoil and is given by a sinusoidal function of time. From Eq. (1), three different cases can be distinguished based on the phase difference ϕ between the pitching angle [Eq. (1)] and the motion of the pitching axis [Eq. (3)]. The three different cases, denoted by MC1, MC2, and MC3, are considered, with phase difference values of 0, 90, and 180 deg, respectively. For the MC1 case (see Fig. 11a), the maximum (minimum) pitching angle is obtained when the instantaneous center of rotation is at the leading (trailing) edge. For the MC2 case (see Fig. 11b), the pitching angle is 0 deg when the instantaneous centers of rotation are located at the leading edge and at the trailing edge. For this case, the maximum and minimum pitching angles are obtained when the center of rotation is at the midchord location. For the MC3 case (see Fig. 11c), the maximum (minimum) pitching angle is obtained when the instantaneous center of rotation is at the trailing (leading) edge.

The average coefficient of lift for the three generalized pitching cases is compared in Table 2. It can be seen from Table 2 that the time-averaged coefficient of lift for the MC2 case is twice the value obtained for the MC1 and MC3 cases, respectively. To study the contribution of the quasi-steady effects to the time-averaged lift, the

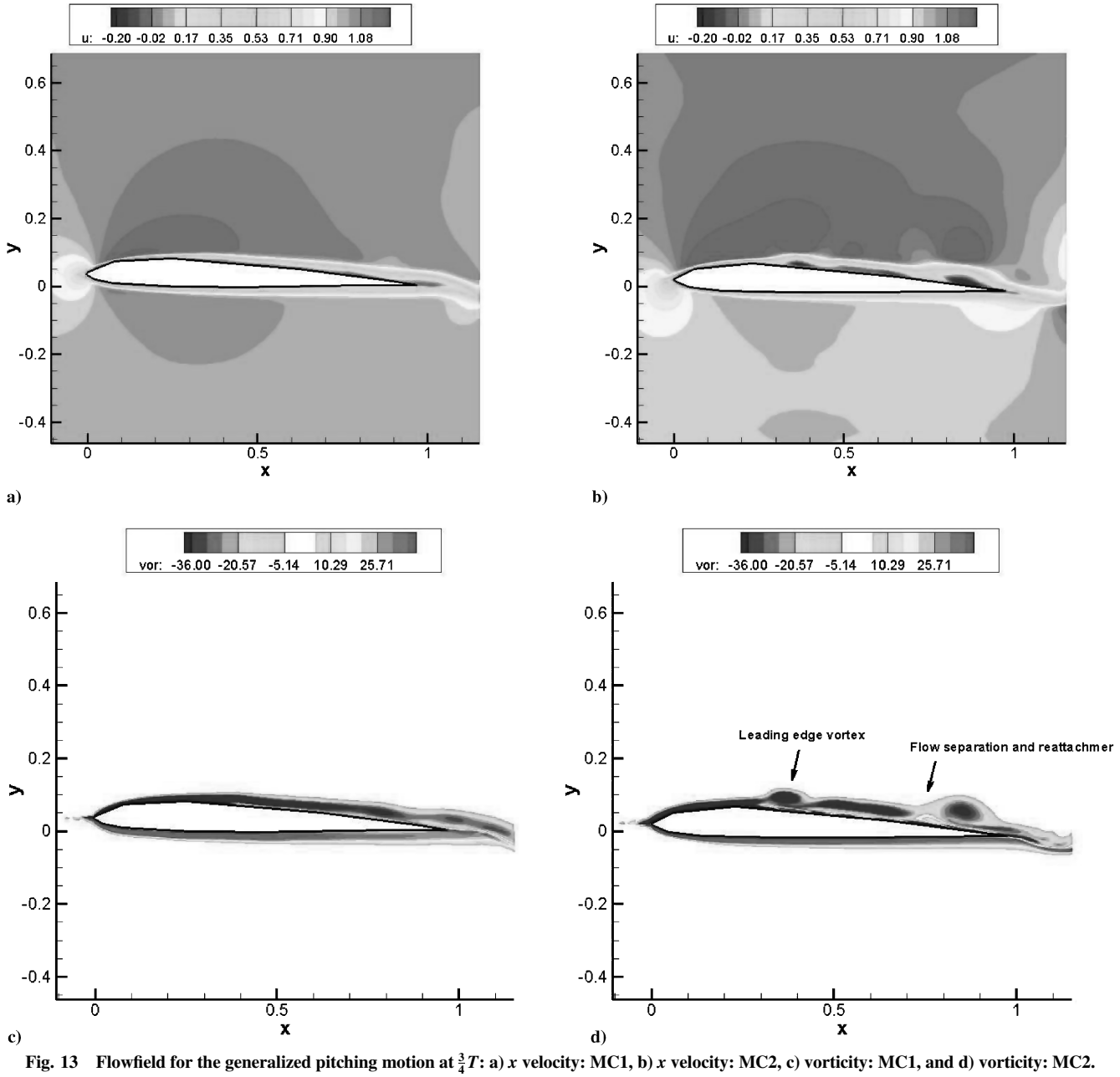

Fig. 13 Flowfield for the generalized pitching motion at $\frac{3}{4}T$: a) x velocity: MC1, b) x velocity: MC2, c) vorticity: MC1, and d) vorticity: MC2.

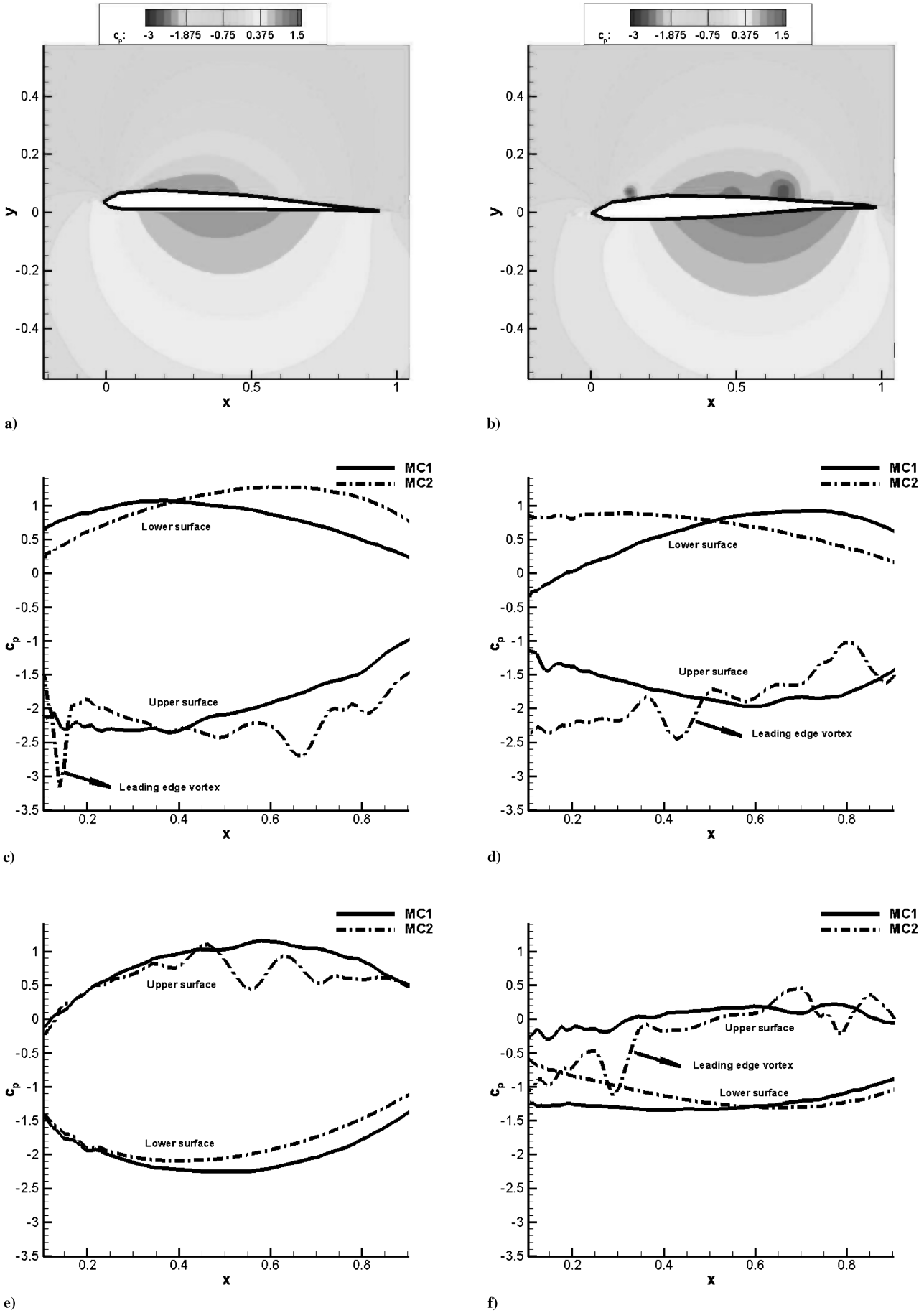

Fig. 14 Comparison of the coefficient of pressure between MC1 and MC2: a) C_p contours: MC1 at time moment corresponding to the local maximum of lift, Max1, b) C_p contours: MC2 at Max1, c) C_p on airfoil surface: Max1, d) C_p: Max2, e) C_p: Min1, and f) C_p: Min2.

plot of the pitching amplitude, location of pitching axis, and coefficient of lift are shown in Figs. 12a–12c, for the MC1, MC2, and MC3 cases, respectively. Two minima and two maxima over a period are caused by interaction of two sinusoidal functions with the same frequency: namely, motion of center of rotation and pitching motion. The pitching angle, axis location, and instantaneous coefficient of lift for all the three cases are given in Table 3. For all the cases, it can be seen that the location and pitching amplitude of the maximum and minimum values of the instantaneous coefficient of lift are approximately symmetric about the half-chord. However, the value of the coefficient of lift is not symmetric, due to the dynamic motion effects. For the MC3 case, the minimum values (denoted as Min1 and Min2 in Fig. 12c) of the instantaneous coefficient of lift are obtained when the airfoil is at the trailing and leading edges, respectively (maximum negative lift). For the MC3 case, maximum pitch rate occurs when the center of rotation is at the vicinity of midchord for both the upstroke and the downstroke phases; therefore, the effects of plunge velocity on lift tend to cancel out. Hence, this can explain the reason for the mean coefficient of lift for the MC3 case being smaller than the MC2 and MC1 case. For the MC1 case, the maximum values (denoted as Max1 and Max2 in Fig. 12a) of the instantaneous coefficient of lift are obtained at the leading and trailing edges, respectively (maximum positive lift). However, the average coefficient of lift for the MC1 case is clearly lower than the MC2 value (see Table 2). Hence, this suggests that the dynamic effect of the airfoil motion is the main factor that results in an increase of the average coefficient of lift for the MC 2 case.

To investigate the reasons for the increase in the average coefficient of lift for the MC2 case, the instantaneous streamwise velocity and vorticity are shown in Fig. 13 at $t = 0.75T$. For the MC1 case, the velocity and vorticity contours show that the flow remains attached to the airfoil everywhere except close to the trailing edge. There is a small area of negative velocity in the flowfield near the trailing edge. For the MC1 case, the LEV is not sustained during the course of motion (see C_p curves for the MC1 case in Fig. 14) and hence the effect of the motion of the pitching axis on the time-averaged coefficient of lift is small (see Table 2, case MC1). For the MC2 case, there is a visible separation of flow at the upper surface of the airfoil and reattachment near $x/c = \frac{3}{4}$ (see Fig. 13d). This cause a significant reduction in the instantaneous pressure field at the upper surface of the airfoil (see Figs. 14a–14f), thereby resulting in the increase of the period-averaged coefficient of lift compare to steady flight (see Table 2). As shown in Fig. 14 for time moments corresponding to maxima and minima of lift, the LEV is sustained during the period of airfoil motion for the MC2 case.

Although the MC2 causes an increase of the average coefficient of lift compared to the steady case, MC1, and MC3, the MC2 case (see Table 2) still does not generate thrust for the considered pitching amplitude. The use of a combined pitch–plunge motion of the airfoil with a phase difference of 90 deg has been commonly used in the literature for generation of thrust [33]. To compare the performance of the MC2 case with this combined motion, a combined pitch–plunge simulation with a phase difference of 90 deg has been performed with a plunging amplitude of $h = 0.035$. This value was chosen to match the maximum displacement of the airfoil during the pitching motion.

The obtained period-averaged coefficients of lift and thrust are shown in Table 2. The combined pitch–plunge motion produces more lift than in all cases of pure pitch with fixed pitching axis presented in Table 1, but much less lift than in the MC2 case. However, the combined pitch–plunge case produces thrust, whereas the MC2 case results in drag. Hence, to investigate the possibility of generating thrust in the MC2 case, further simulations were performed for a combined pitch–plunge motion with the axis moving according to MC2. The mean coefficients of lift and thrust for this motion are given in Table 2. It can be seen that this modified motion produces a higher value of lift force than the MC2 case while generating significant thrust at the same time.

This section is concluded with following observations:

1) Stable LEV causes a higher value of the mean coefficient of lift for the MC2 case compared to the MC1 and MC3 cases.

2) Coefficient of lift for the MC2 case is more than two times higher than that for combined pitch–plunge motion with a phase difference of 90 deg.

3) Combined pitch–plunge motion with a phase difference of 90 deg between them produces thrust, whereas the MC2 case produces drag.

4) MC2 case with an added plunge motion obtains higher mean value of lift than MC2 and produce thrust indicating the possibility of using superposition of kinematics motions of wings to generate the required lift and thrust forces.

VI. Conclusions

The numerical model of aerodynamics of flapping airfoils in generalized pitching motion has been developed based on the high-order finite-difference approximation of derivatives in numerical solution of Navier–Stokes equations in a noninertial coordinate system attached to the moving airfoil. Comparison of numerical results for pitching and plunging motions of the airfoil with the experimental data at $Re = 10,000$ showed good agreement for the streamwise velocity and vorticity, wake velocity profile, and streaklines.

Next, the pure-pitch case was considered for the pitching axis located at different points along the chord. It was observed that the maximum mean coefficient of lift was obtained when the pitching axis was at the leading or trailing edge. The comparison of the CFD results with the quasi-steady expressions showed a good agreement between them. The momentary lift appears to be an order of magnitude higher than steady lift caused by the angle of incidence; however, the time-averaged value of lift is only moderately higher than that for steady flight.

The generalized pitching motion was then studied for three different phase differences between the pitching amplitude and the motion of the axis. It was found that the use of quasi-steady approximation leads to significant error in the estimate of lift coefficient, and therefore CFD computations are essential for the generalized pitching motion of wings. It was found that the maximum mean coefficient of lift was produced when the phase difference was 90 deg. Further, the value of lift was found to be more than doubled compared to that obtained by combined pitch–plunge motion. However, unlike the combined pitch–plunge motion, the generalized pitching motion did not produce thrust.

Finally, a modified kinematic motion that adds a plunging motion to the generalized pitching motion was investigated. It was found that this superposition of the motions increased the value of the lift coefficient compared to a generalized pitching motion. Further, it also generated thrust force as opposed to the generalized pitching motion. Findings of this study support the use of superposition of complex kinematic motions to obtain a needed amount of lift and thrust.

Appendix: Quasi-Steady Approach

In a quasi-steady approach, the coefficient of lift has two contributions: steady-state contribution and contribution from the pitch/plunge motion. The total coefficient of lift can be written as

$$C_L(t) = C_{L0} + C_{L1}(t) \tag{A1}$$

The expression for the steady-state contribution is given by

$$C_{L0} = 2\pi(\alpha_m - \alpha_0) \tag{A2}$$

where α_m is the mean angle of attack and α_0 is the angle of attack for zero lift (-2 deg for the SD 7003 airfoil [25]). The expression for $C_{L1}(t)$ was derived by Garrick [21] and Young [22]. For pure-pitching motion, the expression becomes [22]

$$C_{L1}(t) = C_{L\text{Peak}} \cos(2kt + \phi_L) \tag{A3}$$

where $C_{L\text{Peak}}$ and ϕ_L are given by

$$C_{L\text{Peak}} = 2\pi\theta_0\sqrt{(1+(a-1/2)^2k^2)(F^2+G^2)+k^2/2F+(k+a(a-1/2)k^3)G+1/4(1+a^2k^2)k^2} \quad \text{(A4)}$$

$$\phi_L = \phi + \tan^{-1}\left[\frac{k/2-(a-1/2)kF+G}{ak^2/2+(a-1/2)kG+F}\right] \quad \text{(A5)}$$

where $C(k) = F(k) + iG(k)$ is the Theodorsen function, and $a = 2x_c/c - 1$ is the pivot-point location parameter. The details of expressions for pure plunge and combined pitch–plunge can be found in [21,22].

Acknowledgments

The authors thank the U.S. Air Force Office of Scientific Research (AFOSR) for partial financial support through the AFOSR research grant FA9550-07-0314. The first author thanks the teaching assistantship provided by the Graduate School at the University of Akron. The second author acknowledges the Summer Faculty Fellowship at the U.S. Air Force Research Laboratory (AFRL) at Wright-Patterson Air Force Base (WPAFB), Dayton, OH. The authors thank Michael Ol (AFRL at WPAFB) for valuable discussions and for providing the PIV data for the pure-pitch and pure-plunge cases. The authors would like to thank the Ohio Supercomputing Center for computer time grant to enable access to their computers for performing computations.

References

[1] Mueller, T. J., and DeLaurier, J. D., "Aerodynamics of Small Vehicles," *Annual Review of Fluid Mechanics*, Vol. 35, 2003, pp. 89–111. doi:10.1146/annurev.fluid.35.101101.161102

[2] Shyy, W., Berg, M., and Ljungqvist, D., "Flapping and Flexible Wings for Biological and Micro Air Vehicles," *Progress in Aerospace Sciences*, Vol. 35, No. 5, 1999, pp. 455–505. doi:10.1016/S0376-0421(98)00016-5

[3] Ho, S., Nassef, H., Pornsinsirirak, N., Tai, Y.-C., and Ho, C.-M., "Unsteady Aerodynamics and Flow Control for Flapping Wing Flyers," *Progress in Aerospace Sciences*, Vol. 39, 2003, pp. 635–681. doi:10.1016/j.paerosci.2003.04.001

[4] Pesavento, U., and Wang, J. Z., "Flapping Wing Flight Can Save Aerodynamic Power Compared to Steady Flight," *Physical Review Letters*, Vol. 103, 2009, Paper 118102. doi:10.1103/PhysRevLett.103.118102

[5] Lian, Y., and Shyy, W., "Laminar-Turbulent Transition of a Low Reynolds Number Rigid or Flexible Airfoil," *AIAA Journal*, Vol. 45, No. 7, 2007, pp. 1501–1513. doi:10.2514/1.25812

[6] Ol, M., Parker, G., Abate, G., and Evers, J., "Flight Controls and Performance Challenges for MAVs in Complex Environments," AIAA Guidance, Navigation and Control Conference and Exhibit, Honolulu, HI, AIAA Paper 2008-6508, 18–21 August 2008.

[7] Davis, W. R., Kosicki, B. B., Boroson, M. D., and Kostishack, D. F., "Micro Air Vehicles for Optical Surveillance," *Lincoln Laboratory Journal*, Vol. 9, No. 2, 1996, pp. 197–214.

[8] Mueller, T. J. (ed.), *Fixed and Flapping Wing Aerodynamics for Micro Air Vehicle Applications*, AIAA Progress in Astronautics and Aeronautics, Vol. 195, AIAA, Reston, VA, 2001.

[9] Ellington, C. P., "The Novel Aerodynamics of Insect Flight: Application to Microair Vehicles," *Journal of Experimental Biology*, Vol. 202, No. 23, 1999, pp. 3439–3448.

[10] Jones, K., and Platzer, M., "Bio-Inspired Design of Flapping Wing Micro Air Vehicles—An Engineer's Perspective," 44th AIAA Aerospace Sciences Meeting and Exhibit, Reno, NV, AIAA Paper 2006-37, 9–12 Jan. 2006.

[11] Gad-el-hak, M., "Micro-Air-Vehicles: Can They Be Controlled Better," *Journal of Aircraft*, Vol. 38, No. 3, 2001, pp. 419–429. doi:10.2514/2.2807

[12] Lian, Y., and Shyy, W., "Aerodynamics of low Reynolds number plunging airfoil under gusty environment," *45th AIAA Aerospace Sciences Meeting and Exhibit*, Reno, NV, AIAA Paper 2007-794, 8–11 Jan. 2007.

[13] Webb, C., Dong, H., and Ol, M., "Effects of Unequal Pitch and Plunge Airfoil Motion Frequency on Aerodynamic Response," 46th AIAA Aerospace Sciences Meeting and Exhibit, Reno, NV, AIAA Paper 2008-582, 7–10 Jan. 2008.

[14] Anderson, J. M., Streitlien, D., Barrett, D. S., and Triantafyllou, M. S., "Oscillating Foils of High Propulsive Efficiency," *Journal of Fluid Mechanics*, Vol. 360, 1998, pp. 41–72. doi:10.1017/S0022112097008392

[15] Read, D. A., Hover, F. S., and Triantafyllou, M. S., "Forces on Oscillating Foils for Propulsion and Maneuvering," *Journal of Fluids and Structures*, Vol. 17, 2003, pp. 163–183. doi:10.1016/S0889-9746(02)00115-9

[16] Isogai, K., Shinmoto, Y., and Watanabe, Y., "Effects of Dynamic Stall on Propulsive Efficiency and Thrust of Flapping Airfoil," *AIAA Journal*, Vol. 37, 1999, pp. 1145–1151. doi:10.2514/2.589

[17] Ramamurti, R., and Sandberg, W., "Simulation of Flow About Flapping Airfoils Using Finite Element Incompressible Flow Solver," *AIAA Journal*, Vol. 39, 2001, pp. 253–260. doi:10.2514/2.1320

[18] Schouveiler, L., Hover, F. S., and Triantafyllou, M. S., "Performance of flapping foil propulsion," *Journal of Fluids and Structures*, Vol. 20, No. 7, 2005, pp. 949–959. doi:10.1016/j.jfluidstructs.2005.05.009

[19] Sane, P. S., "The Aerodynamics of Insect Flight," *Journal of Experimental Biology*, Vol. 206, 2003, pp. 4191–4208. doi:10.1242/jeb.00663

[20] Jones, K. D., Lund, T. C., and Platzer, M. F., "Experimental and Computational Investigation of Flapping-Wing Propulsion for Micro Air Vehicles," *Fixed and Flapping Wing Aerodynamics for Micro Air Vehicle Applications*, AIAA Progress in Aerospace Sciences Series, Vol. 195, edited by T. Mueller, 2001, pp. 307–339.

[21] Garrick, I., "Propulsion of a Flapping and Oscillating Airfoil," NACA Rept. 537, 1936.

[22] Young, J., "Numerical Simulation of the Unsteady Aerodynamics of Flapping Airfoils," Ph.D. Dissertation, Univ. of New South Wales, Australian Defence Force Academy, School of Aerospace, Civil and Mechanical Engineering, Canberra, Australia, 2005.

[23] Gopalan, H., "Numerical Modeling of Aerodynamics of Airfoils of Micro Air Vehicles in Gusty Environment," Ph.D. Dissertation, Department of Mechanical Engineering, Univ. of Akron, Akron, OH, 2008.

[24] Gopalan, H., and Povitsky, A., "Short Communication: Stream-function-Potential Function Coordinates for Computational Aeroacoustics," *International Journal of Computational Fluid Dynamics*, Vol. 23, No. 3, 2009, pp. 285–290. doi:10.1080/10618560902798079

[25] McGowan, G., Gopalarathnam, A., Ol, M., and Edwards, J., "Analytical, Computational, and Experimental Investigations of Equivalence Between Pitch and Plunge Motions for Airfoils at Low Reynolds Numbers," 47th AIAA Aerospace Sciences Meeting, Orlando, FL, AIAA Paper 2009-0535, Jan. 2009.

[26] Lele, S. K., "Compact Finite Difference Scheme with Spectral Like Resolution," *Journal of Computational Physics*, Vol. 103, No. 1, 1992, pp. 16–42. doi:10.1016/0021-9991(92)90324-R

[27] Visbal, M. R., and Gaitonde, D. V., "Very High-Order Spatially Implicit Schemes for Computational Acoustics on Curvilinear Meshes," *Journal of Computational Acoustics*, Vol. 9, No. 4, 2001, pp. 1259–1286. doi:10.1142/S0218396X01000541

[28] Williamson, J. H., "Low-Storage Runge–Kutta Schemes," *Journal of Computational Physics*, Vol. 35, 1980, pp. 48–56. doi:10.1016/0021-9991(80)90033-9

[29] Edgar, N., and Visbal, M. R., "A General Buffer Zone-Type Nonreflecting Boundary Condition for Computational Aeroacoustics," 9th AIAA/CEAS Aeroacoustics Conference and Exhibit, Hilton Head, SC, AIAA Paper 2003-3300, May 2003.

[30] McGowan, G., Gopalarathnam, A., Ol, M., Edwards, J., and Fredberg, D., "Computation vs. Experiment for High-Frequency Low-Reynolds Number Airfoil Pitch and Plunge," 46th AIAA Aerospace Sciences Meeting and Exhibit, Reno, NV, AIAA

Paper 2008-0653, 7–10 Jan. 2008.
[31] Selig, M. S., Guglielmo, J. J., Broeren, A. P., and Giguere, P., *Summary of Low-Speed Airfoil Data*, Vol. 1, SoarTech, Virginia Beach, VA, 1995.
[32] Ol, M. V., McAuliffe, B. R., Hanff, E. S., Scholz, U., and Kahler, C., "Comparison Of Laminar Separation Bubble Measurements on a Low Reynolds Number Airfoil in Three Facilities," 35th AIAA Fluid Dynamics Conference and Exhibit, Toronto, AIAA Paper 2005-5149, June 2005.
[33] Sarkar, S., and Venkatramam, K., "Numerical Simulation of Thrust Generating Flow Past a Pitching Airfoil," *Computers and Fluids*, Vol. 35, No. 1, 2006, pp. 16–42.
doi:10.1016/j.compfluid.2004.10.002